THE JOURNAL OF PHYSICAL CHEMISTRY C

Article

pubs.acs.org/JPCC

In Situ Observation of Melting Behavior of ZnTe Nanowires

Mehrdad Shaygan,[†] Thomas Gemming,[‡] Viktor Bezugly,[§] Gianaurelio Cuniberti,[§] Jeong-Soo Lee,[†] and M. Meyyappan*,[∥]

[†]Department of IT Convergence Engineering, Pohang University of Science and Technology, Pohang, South Korea

[‡]IFW Dresden, P.O. Box 270116, D-01171 Dresden, Germany

[§]Institute for Materials Science and Max Bergmann Center of Biomaterials, TU Dresden, 01062 Dresden, Germany

[∥]NASA Ames Research Center, Moffett Field, California 94035, United States

ABSTRACT: The melting behavior of ZnTe nanowires has been investigated using a transmission electron microscope in both bright field and high-angle annular dark field modes. The ZnTe nanowires, 30−160 nm in diameter, were heated using a controllable heating system, and their melting temperature was studied. The results showed a significant reduction of the melting temperature of about 450 °C, depending on the diameter of the nanowire, compared to the bulk melting point of 1300 °C. In addition, scanning transmission electron microscopy using high-angle annular dark field imaging was carried out to structurally analyze the ZnTe nanowires after melting.

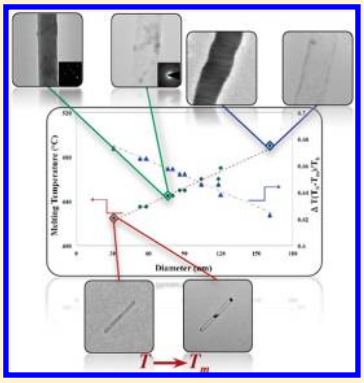

1. INTRODUCTION

One-dimensional (1D) nanostructures such as wires, rods, belts, ribbons, and tubes have attracted a great deal of attention in the fabrication of nanoscale devices, and the size-dependent properties of various inorganic nanowires have been studied to promote applications.[1−3] Semiconductor nanowires prepared by various growth techniques have many applications in nanoelectronics, light emitters, photovoltaics, thermoelectrics, energy storage devices, and biosensors.[1] Employing the nanowires as building blocks for nanoscale electronics warrants consideration of the relevant thermodynamic properties due to their dependency on low dimensionality and large surface area.[4] The melting temperature of nanomaterials as one of the basic thermodynamic properties has been studied and compared with bulk melting point for some nanowires,[5−7] nanoparticles,[8,9] and nanorods.[10,11] The thermal behavior of nanostructures in nanoelectronics and other applications plays a key role in their function influencing their performance and reliability. Therefore, their melting temperature should be investigated in order to avoid melting or partial melting of these active components during the lifetime of the devices.

Generally, the melting point of the nanomaterials decreases with a reduction in size compared to the bulk material. For example, Hui et al.[7] employed molecular dynamic simulations to study the melting behavior of a Zr nanowire and found it to melt at 900 K, compared to the bulk melting point of 2125 K. Pan et al.[12] reported partial melting of a submicrometer-sized grain of iron at 650 °C, which is significantly lower than the melting temperature of bulk Fe at 1536 °C. Size dependency of melting point in Ga clusters has been reported by Breaux et al.,[13] where size reduction lead to a higher melting point than the bulk material. The investigation of the melting temperature in nanowires has focused more on metals than semiconductors, except for a few reports. A marked reduction in melting temperature of 10−100 nm diameter Ge nanowires was observed at 650 °C for nanowires versus 930 °C for bulk material.[14] A similar suppressing trend in melting point of In_2Se_3 nanowires has been reported at 680 °C compared to the bulk melting temperature of 890 °C.[5] A 46% reduction in melting temperature was reported for 40−80 nm diameter GeTe nanowires for their use in phase change random-access memory application.[6] Differential scanning calorimetry (DSC)[15,16] and transmission electron microscopy (TEM)[5,6] have been typically used in the nanomaterial melting behavior studies. TEM as a standard tool to investigate the melting behavior of a nanomaterial was first reported by Takagi.[17] In situ TEM has been previously utilized as a powerful tool for atomic-level observation of phase transformation,[18] welding of nanostructures,[14] electromigration,[19] nano-heterostructure growth,[20] and nanodevice fabrication.[21]

ZnTe is a II−VI semiconductor with a direct bandgap of 2.26 eV at room temperature and a Bohr radius of 6.2 nm. ZnTe has been considered for optoelectronic devices such as green light-emitting diodes,[22] photovoltaics,[23] electro-optic devices,[24] visible-light photodetectors,[25] and thermoelectric devices.[26] Given the wide range of applications, the melting behavior of ZnTe is of interest, and here, we present the results from our

Received: April 3, 2014
Revised: May 27, 2014
Published: June 9, 2014

dx.doi.org/10.1021/jp503312z | J. Phys. Chem. C 2014, 118, 15061−15067

study on the size-dependent melting behavior of ZnTe nanowires using in situ transmission electron microscopy.

2. EXPERIMENTAL WORK

The ZnTe nanowires were grown on silicon substrates covered with a 3 nm gold layer via the vapor−liquid−solid technique, as described in detail in ref 27. The nanowires were dispersed in ethanol using an ultrasonic technique and the droplets of the dispersion were deposited on a copper grid with a holey carbon film, which was mounted in the heating stage holder. The as-grown ZnTe nanowires were imaged with a scanning electron microscope (SEM) (JEOL JSM-7401F) to study the morphology. Transmission electron microscopy (TEM) images in both bright and dark field modes (BF, HAADF-STEM) were recorded using a Tecnai F30 (FEI) scanning transmission electron microscope (STEM) operated at 300 kV equipped with electron energy loss spectrometer (EELS) and energy dispersive X-ray spectrometer (EDXS) to determine the chemical composition. The isothermal in situ heating experiments were performed using a Gatan heating holder. A one-minute waiting time was considered before recording data to allow for the stabilization of the target temperature. The real-time melting behavior and monitoring the morphology of the nanowires were investigated in the bright-field mode. The sample stage was resistively heated during the experiments in 50 °C steps from room temperature to 375 and 5 °C steps from 375 to 520 °C, while the heating rate ranged from 10 to 20 °C/min.

3. RESULTS AND DISCUSSION

Electron microscopy images of ZnTe nanowires grown by the VLS technique are shown in Figure 1. The mat of nanowires shows a high-yield with diameters in the range of 30−120 nm and several micrometers in length (Figure 1a). Figure 1b shows a higher magnification SEM image of a single ZnTe nanowire with a diameter of 72 nm. A low-magnification TEM image of a nanowire with a uniform diameter of 63 nm is shown in Figure 1c. The EDXS analysis of a single nanowire (not shown here) confirmed the composition of the nanowire of only zinc and tellurium with an atomic ratio of 1:1. The TEM images in Figure 1 (panels c and d) reveal that the nanowire has a crystalline FCC lattice structure, which is uniform with a regular stacking fault structure. The measured lattice spacing of the grown ZnTe nanowire of 0.35 nm is in good agreement with the *d*-spacing of the (1 1 1) plane of ZnTe structure. The growth direction of the nanowire was determined as <1 1 1> by using the selected area diffraction pattern (SAD) (not shown here) being indexed to the cubic FCC structure.

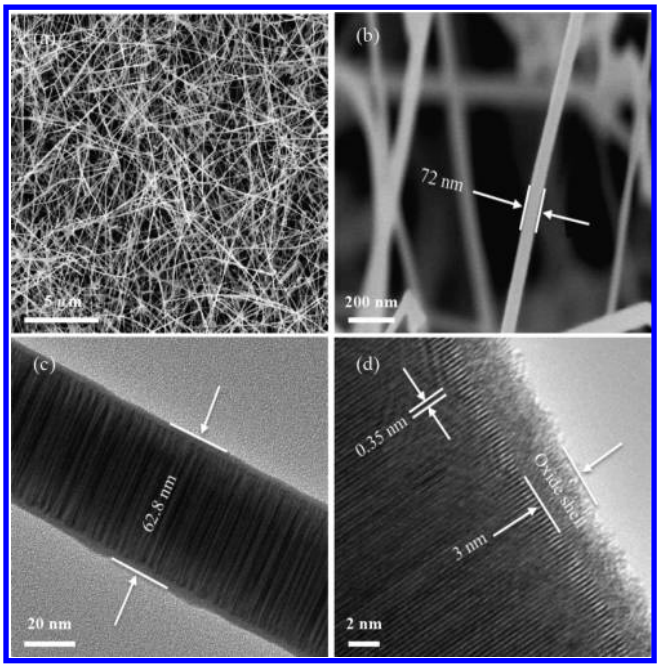

Figure 1. (a) SEM image of a mat of high-yield ZnTe nanowires grown by VLS technique. (b) Higher magnification SEM image of an individual ZnTe nanowire. (c) Low-magnification TEM image of a single ZnTe nanowire. (d) High-resolution TEM image of a ZnTe nanowire, showing a 3 nm oxide shell around the nanowire.

A ∼3 nm native oxide was inevitably formed on the surface of the nanowire and could be due to exposure to the ambient environment right after the synthesis or oxygen leakage during growth. The composition of this layer has been determined as ZnO by Kirmse et al.[28] with a speculation of its origin as the post-growth formation due to the absence of oxygen in their molecular beam epitaxy system. Our investigation by local electron energy loss spectroscopy (EELS) confirmed the oxide composition of this layer (as discussed later). The selected area diffraction pattern is used here to define the melting temperature T_m of the nanostructure. The temperature corresponding to the disappearance of electron diffraction peaks associated with the solid phase is defined as the melting temperature of the solid nanostructure.[8] Figure 2 exhibits

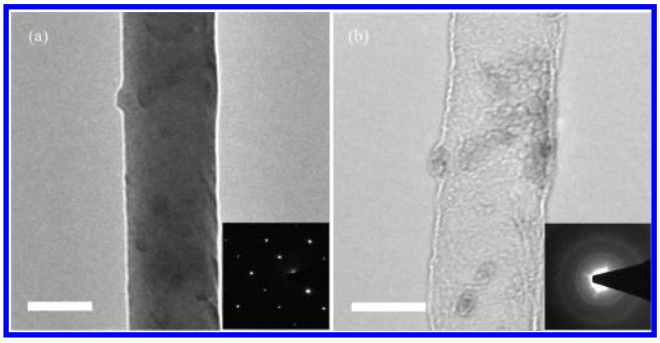

Figure 2. Melting process of an individual ZnTe nanowire during in situ heating and monitored by TEM. (a) The ZnTe nanowire at room temperature. Inset: the correspondent SAD pattern shows the crystalline structure of the nanowire. (b) The molten nanowire at 445 °C. The remaining oxide shell can be clearly seen from the image. The inset shows the SAD pattern without crystalline reflections. All scale bars are 50 nm.

sequential TEM images during the melting process of a 70 nm ZnTe nanowire. The electron diffraction pattern (shown in the inset) before the commencing of the heating confirms the crystalline structure of the ZnTe nanowire. The melting process was started by heating the holder stage resistively at a rate of 10 °C/min, while monitoring the phase transformation of ZnTe nanowire from solid crystalline phase to the liquid phase. The melting point of this ZnTe nanowire was determined to be 445 °C from the characteristic vanishing of the crystalline reflections of the SAD pattern shown in the inset of Figure 2b.

Figure 3 shows low-magnification TEM images of ZnTe nanowires with two different diameters (74.2 and 30.6 nm) during the melting process. The TEM images at 160 and 320 °C show that the nanowires still remain in the solid phase

dx.doi.org/10.1021/jp503312z | J. Phys. Chem. C 2014, 118, 15061−15067

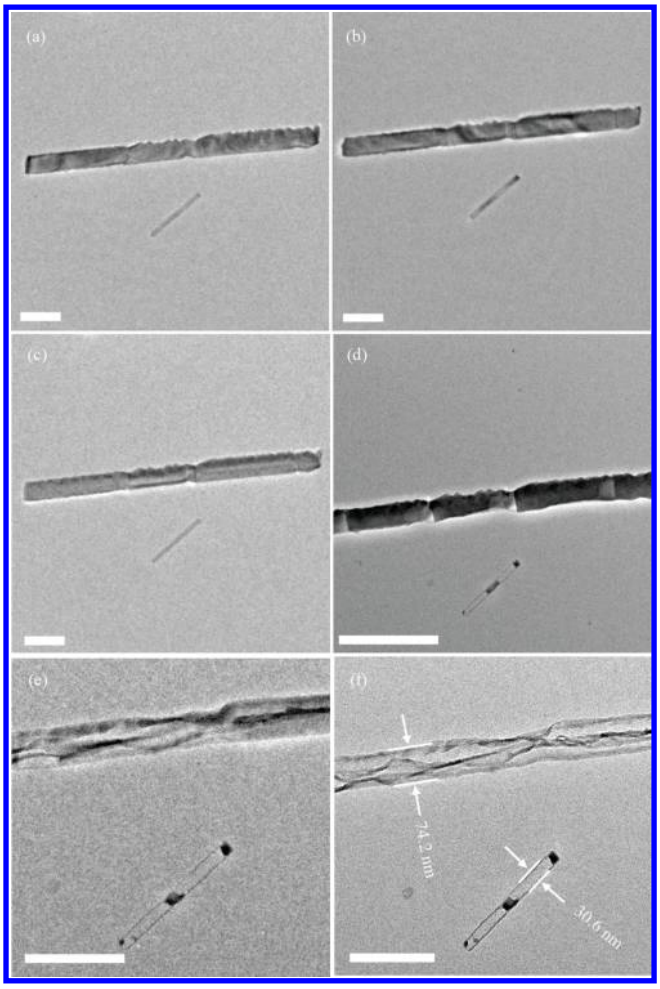

Figure 3. Low-magnification TEM images of two ZnTe nanowires (diameters of 31 and 74) taken in a wide range of temperatures to study their melting behavior. (a–e) Different steps of the melting process at room temperature, 160, 320, 425, and 450 °C, respectively. (f) The final step of the melting process of the molten nanowires with a diameter of 31 and 74 nm. All scale bars are 200 nm.

(Figure 3, panels b and c). The smaller nanowire with a diameter of 31 nm started to melt at 425 °C, but the larger one still remains solid at this stage (Figure 3d). The melting of the ZnTe nanowire seems to initiate from the middle part of the nanowire at kinks. However, the nanowire melting process is generally thought to start at the two ends, where the melting point is the lowest probably due to the highest curvature.[14] Figure 3e shows the melting of the larger nanowire at 450 °C, while the final step of the melting of both nanowires results in only the empty oxide shell (Figure 3f).

Further STEM investigation was conducted in order to study the chemical composition of the very thin shell around the nanowire in Figure 3f. Figure 4a shows a high-angle annular dark field-STEM image of a 35 nm diameter nanowire. Elemental profiles across the melted ZnTe nanowire were measured by scanning a finely focused electron probe across the structure and recording EEL spectra at each position. A set of 41 EEL spectra was acquired across the nanowire marked with the red line in the STEM dark-field image (Figure 4a) with a spatial step size of about 1.5 nm. An example of the oxygen-K edge measured at the shell[29] is shown in Figure 4b, which is in good agreement for the EELS result for ZnTe nanowires.[28]

Figure 4c shows the HAADF-STEM brightness across the whole diameter of the nanowire, where the brightness difference indicates the presence of different elements based on different atomic numbers. The distribution of oxygen on the sidewall of ZnTe nanowire across its diameter is displayed in Figure 4d. Oxygen was detected significantly at the two outer areas of the nanowire (16 and 45 nm), indicating the oxide composition of the shell. Since the melting temperature of bulk ZnO (1976 °C) is higher than that of bulk ZnTe (1300 °C), only the ZnO shell remained when the temperature rose up to the melting temperature of ZnTe nanowire. The melting temperature of ZnO nanorods has been reported as 750 °C, which is significantly lower than that of bulk material but still higher than that of the ZnTe nanowire.[10]

A similar trend of reduction in melting temperature of nanomaterials with comparable configurations has been reported by other groups. Huang et al.[30] monitored the melting behavior of a 50 nm diameter ZnO nanowire covered by an alumina shell structure where the ZnO nanowire started to melt at 600 °C, far from the bulk melting temperature of zinc oxide. They surmised that the alumina shell around the ZnO nanowire acted as a heating barrier withstanding the heating while the inner core melted. A high suppression of melting temperature compared to the bulk material was also observed for Ge nanowires encapsulated in the carbon nanotube,[14] where the initial and final melting temperature dropped 120–300 °C and 50–200 °C, respectively, from that of the bulk value.

A STEM image of a ZnTe nanowire after completion of the melting process is shown in Figure 5a, and the sphere-shaped bright spot in the image was confirmed as gold by EDAX analysis (Figure 5b). The existence of the catalyst bead in the VLS-grown nanowires is well-known,[27] and here, the gold nanoparticle (92 nm diameter) was intact during the melting process of the ZnTe nanowire due to its high melting temperature. The melting temperature of the gold in bulk material is 1064 °C, while the size dependency melting behavior of gold nanoparticles is observable below 10 nm.[31] The EDAX results for the catalyst particle do not show any Zn or Te, indicating that no dissolved residuals remained in the particle leading to volume and diameter expansion.

The results show that ZnTe nanowires melt around 450 °C, which is 65% less than the bulk melting temperature of ZnTe (1300 °C). As seen in Figure 6, the melting temperature reduces from 490 to 425 °C by decreasing the diameter of the nanowires from 160 to 31 nm. Many models, including the classical thermodynamic model,[8] surface-phonon instability model,[32] and liquid-drop model,[33] have been introduced to describe the size-dependent behavior of the melting temperature of nanomaterials since the pioneering work by Pawlow[34] in 1909. Interestingly, the predicted values of melting temperature of nanoparticles by Pawlow were much higher than the experimental measurements.[35] Nanda et al.[33] introduced the liquid-drop model, suggesting the size dependency of melting temperature based on the relation between surface energy and cohesive energy. Considering the volume and surface energy of atoms, the cohesive energy of N-atom nanoparticle of diameter d can be written as

$$a_{\upsilon,d} = a_{\upsilon} - \frac{6\upsilon_0\gamma}{d} \quad (1)$$

where $a_{\upsilon,d}$ and a_{υ} represent the corresponding cohesive energies for the nanoparticle per atom and bulk, respectively, υ_0 is the atomic volume, and γ is the surface energy of the solid–vapor

dx.doi.org/10.1021/jp503312z | J. Phys. Chem. C 2014, 118, 15061–15067

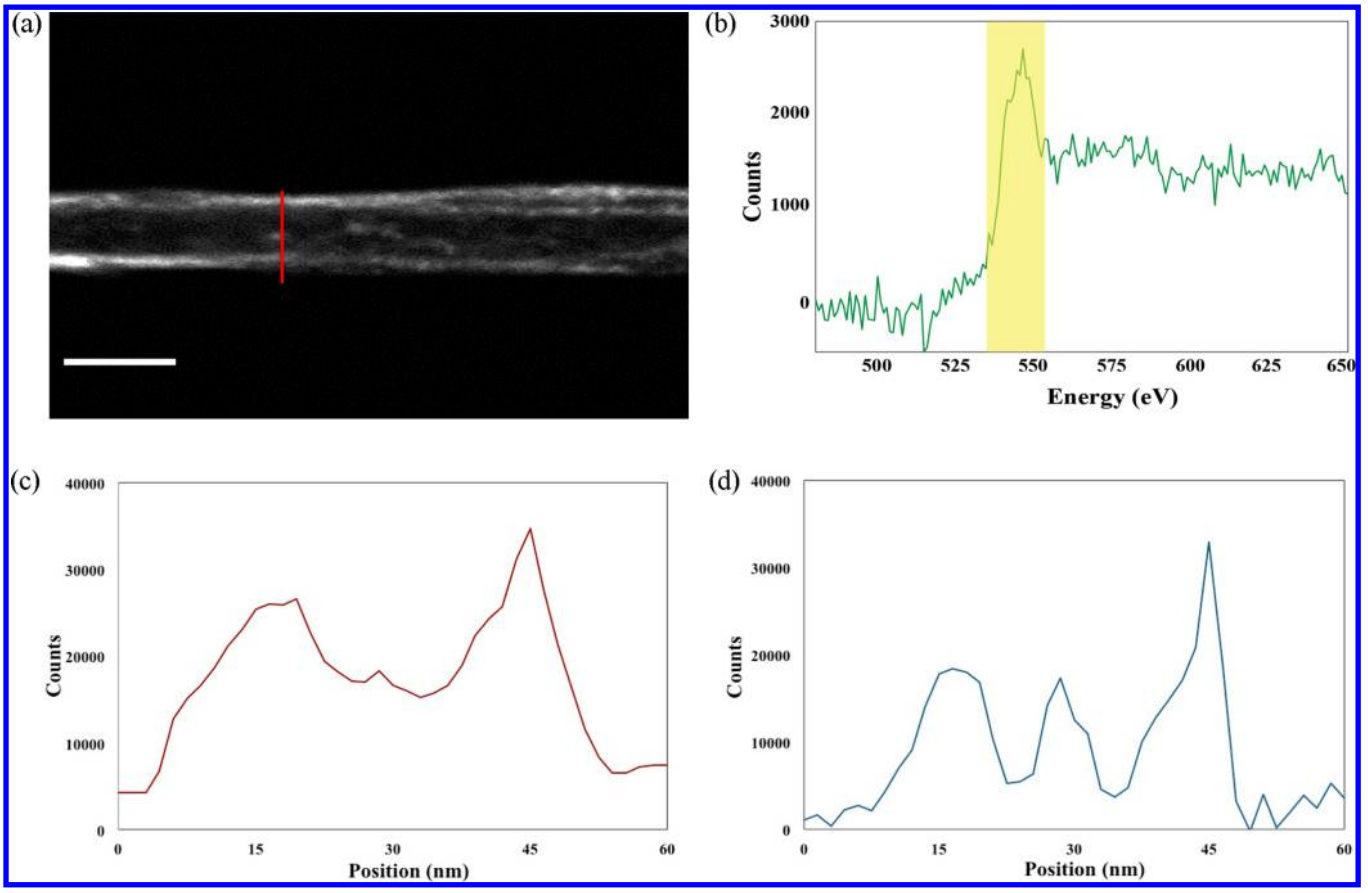

Figure 4. (a) A high-angle annular dark field (HAADF)-STEM image of a ZnTe nanowire after melting. The scale bar is 50 nm. (b) Measured EELS O K-edge at the shell around the ZnTe nanowire. (c) The brightness profile of the HAADF-STEM image along the red line shown in (a). (d) EELS line scan along the red line across the ZnTe nanowire shown in (a).

interface. By employing the empirical relations, the melting temperature of nanoparticle ($T_{m(NP)}$) in terms of bulk melting temperature (T_{mb}) can be expressed as

$$\frac{T_{m(NP)}}{T_{mb}} = 1 - \frac{6\upsilon_0}{0.0005736d}\left(\frac{\gamma}{T_{mb}}\right) = 1 - \left(\frac{\beta}{d}\right) \quad (2)$$

where

$$\beta = \frac{6\upsilon_0}{0.0005736d}\left(\frac{\gamma}{T_{mb}}\right)$$

In the case of spherical particles with a diameter (d), the relevant melting temperature after substituting the surface-to-volume ratio ($A = 6/d$) can be expressed as

$$\frac{T_{m(NP)}}{T_{mb}} = 1 - \frac{\beta}{6}A \quad (3)$$

For a cylindrical particle with height of l and diameter d, the surface-to-volume ratio is ($A = 4/d + 2/l$), which when substituted in eq 3 gives

$$\frac{T_{m(NP)}}{T_{mb}} = 1 - \frac{\beta}{6}\left(\frac{4}{d} + \frac{2}{l}\right) \quad (4)$$

The melting temperature ($T_{m(NW)}$) of a thin wire with $l \gg d$, employing the same model, is given by

$$\frac{T_{m(NW)}}{T_{mb}} = 1 - \frac{2\beta}{3d} \quad (5)$$

Alternative models based on thermodynamic considerations and simple energy balance provide a relationship for melting point reduction $\Delta\theta$ as,

$$\Delta\theta = \frac{\sigma T_b}{L\rho} \times \frac{1}{\gamma}\left(1 + \frac{1}{AR}\right) \quad (6)$$

where σ is the surface tension of the nanowire, ρ is the nanowire density, L is the latent heat of fusion, and AR is the nanowire aspect ratio. Unfortunately, it is often hard to compare measurements against any of these predictions due to a lack of knowledge of nanowire properties needed in the above relations. The use of available values for bulk ZnTe provides poor predictions substantially different from measurements.

The surface energy plays a key role in determining some macroscopic properties such as thermal stability. In accordance with the thermodynamic model for the surface energy of a nanowire proposed by Quyang et al.,[36,37] the surface energy of a nanowire (γ) consists of structural and chemical contributions, namely, $\gamma = \gamma^{stru} + \gamma^{chem}$, where the structural component is related to the density of surface strain energy and the chemical component is related to the surface atomic dangling bond energy.[36] The structural part of surface energy of a nanowire is given by

$$\gamma^{stru} = \frac{1}{2}\{K_1(\varepsilon_x^{s^2} + \varepsilon_y^{s^2}) + K_2[(\varepsilon_x^s + \varepsilon_y^s)^2 + 4\varepsilon_{xy}^{s^2}]\} \quad (7)$$

dx.doi.org/10.1021/jp503312z | J. Phys. Chem. C 2014, 118, 15061−15067

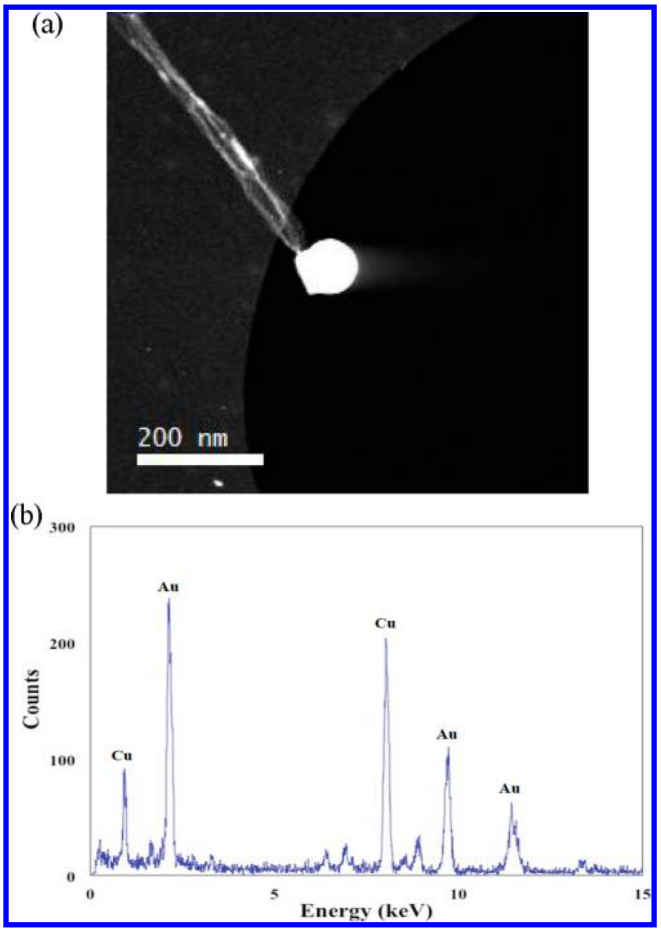

Figure 5. HAADF-STEM image of the molten ZnTe nanowire. The white part on the tip of the nanowire is an Au catalyst [confirmed by the EDAX analysis shown in (b)].

where K is the surface spring coefficient and ε is the surface strain. The chemical part of the surface energy of a nanowire is given by

$$\gamma^{\text{chem}} = \Gamma_{(\text{hkl})}\left(1 - \frac{3h}{d - 3h}\right)\exp\left(-\frac{2S_{\text{mb}}}{3R}\frac{3h}{d - 3h}\right) \quad (8)$$

where $\Gamma_{(\text{hkl})} = [1 - (Z_s/Z_b)^{1/2}]E_B$, in which Z_s, Z_b, and E_B are the coordination number (CN), the bulk one, and the cohesive energy, d is the nanowire diameter, h is the atomic diameter, R is the ideal gas constant, and S_{mb} is the melting entropy. As seen from these relations, the surface energy of nanowires exhibits a size-dependent trend, leading to size-dependent melting temperature of the nanowires.[36]

On the other hand, the under-coordinated atoms at the surface of nanosolids have different bond interaction energies compared to the bulk interior. Generally, the required energy for breaking the atoms of the solid into isolated pieces is defined as the cohesive energy of a solid, in which the atomic cohesive energy is related to the single bond energy in bulk with a portion of atomic coordination numbers ($E_C = zE_B$, where z and E_B are the atomic CNs and single bond energy in bulk, respectively). For a core−shell configuration of a nanostructure with a diameter D containing N atoms, the cohesive energy with pressure and temperature approach can be expressed as[38]

$$E_C(D, p, T) = \sum_{i<3} N_i z_i E_i^s + z_b E_B\left(N - \sum_{i<3} N_i\right) \quad (9)$$

where z_i and z_b are the CN of the i_{th} atomic layer and core bulk, E_i^s is the single bond energy in the surface shell, and N_i is the number of atom in surface shell. On the basis of this model, apparent reduction in CN cannot occur for the core part ($i > 3$). By reducing the CN, the radius of the atoms would shrink and the bonds of the under-coordinated atoms will be shortened by the CN imperfection.[38] In other words, the CN of a surface atom decreases when the remaining bonds of the lower-coordinated surface atoms relax spontaneously. This would affect the atomic cohesive energy, since it can be derived by multiplying the single bond energy and the CN.[39] The CN imperfection could be attributed to the presence of defects at the interface of the core and shell structure,[40] and this could happen here at the interface of the ZnTe core and ZnO shell in our core/shell structure. Hence, the size-dependent behavior of the surface energy of a nanowire and the reduced atomic cohesive energy of ZnTe core and ZnO shell can contribute to the suppressed melting temperature of ZnTe nanowires.

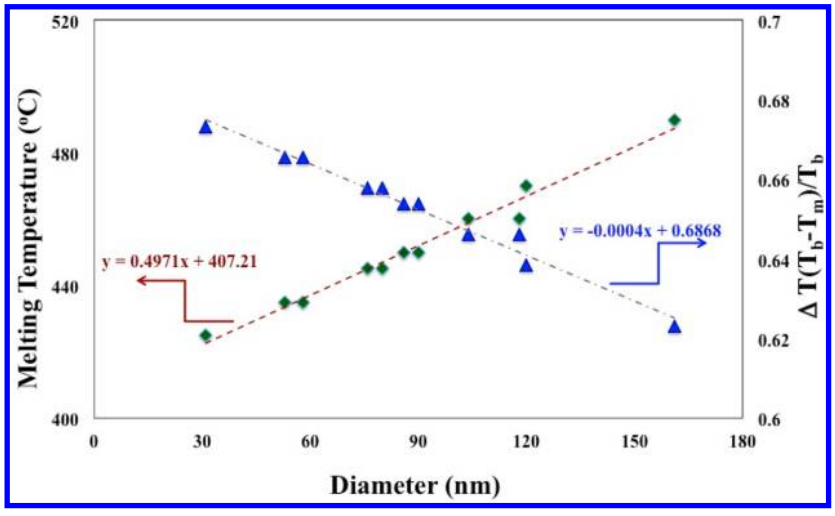

Figure 6. Measured melting temperature and the melting point suppression of ZnTe nanowires as a function of nanowire diameter.

dx.doi.org/10.1021/jp503312z | J. Phys. Chem. C 2014, 118, 15061−15067

4. CONCLUSION

The melting temperature of ZnTe nanowires of varying diameters was investigated using in situ TEM measurements. The composition of the shell around the ZnTe nanowire was confirmed by STEM-EELS to be zinc oxide. A significant decrease in melting temperature by about 65% was observed for the nanowires compared to the bulk material, and the extent of melting point suppression depends on the nanowire diameter.

AUTHOR INFORMATION

Corresponding Author

*E-mail: m.meyyappan@nasa.gov. Tel: +1 (650) 604-2616.

Notes

The authors declare no competing financial interest.

ACKNOWLEDGMENTS

The World Class University program funded by the Ministry of Education, Science and Technology through the National Research Foundation of Korea (R31-10100) supported this research. M.S. did the measurement part of this work during his visit at TUD, and the authors wish to acknowledge Dr. Jurgen Thomas for his helpful support during the measurement.

REFERENCES

(1) Meyyappan, M.; Sunkara, M. *Inorganic Nanowires: Applications, Properties and Characterization*; CRC Press: Boca Raton, FL, 2010.

(2) Xia, Y.; Yang, P.; Sun, Y.; Wu, Y.; Mayers, B.; Gates, B.; Yin, Y.; Kim, F.; Yan, H. One-Dimensional Nanostructures: Synthesis, Characterization, and Applications. *Adv. Mater.* **2003**, *15*, 353−389.

(3) Davami, K.; Weathers, A.; Kheirabi, N.; Mortazavi, B.; Pettes, M. T.; Shi, L.; Lee, J. S.; Meyyappan, M. Thermal Conductivity of ZnTe Nanowires. *J. Appl. Phys.* **2013**, *114*, 134314.

(4) Lu, H. M.; Han, F. Q.; Meng, K. X. Size-Dependent Thermodynamic Properties of Metallic Nanowires. *J. Phys. Chem. B* **2008**, *112*, 9444−9448.

(5) Sun, X.; Yu, B.; Ng, G.; Nguyen, T. D.; Meyyappan, M. III-VI Compound Semiconductor Indium Selenide (In_2Se_3) Nanowires: Synthesis and Characterization. *Appl. Phys. Lett.* **2006**, *89*, 233121.

(6) Sun, X.; Yu, B.; Ng, G.; Meyyappan, M. One-Dimensional Phase Change Nanostructure: Germanium Telluride Nanowire. *J. Phys. Chem. C* **2007**, *111*, 2421−2425.

(7) Hui, L.; Wang, B. L.; Wang, J. L.; Wang, G. H. Melting Behavior of One-Dimensional Zirconium Nanowire. *J. Chem. Phys.* **2004**, *120*, 3431−3438.

(8) Goldstein, A. N.; Echer, C. M.; Alivisatos, A. P. Melting in Semiconductor Nanocrystals. *Science* **1992**, *256*, 1425−1427.

(9) Buffat, Ph.; Borel, J. P. Size Effect on the Melting Temperature of Gold Particles. *Phys. Rev. A* **1976**, *13*, 2287−2298.

(10) Su, X.; Zhang, Z.; Zhu, M. Melting and Optical Properties of ZnO Nanorods. *Appl. Phys. Lett.* **2006**, *88*, 061913.

(11) Link, S.; Wang, Z. L.; El-Sayed, M. A. How Does a Gold Nanorod Melt? *J. Phys. Chem. B* **2000**, *104*, 7867−7870.

(12) Pan, C.; Zhang, Z.; Su, X.; Zhao, Y.; Liu, J. Characterization of Fe Nanorods Grown Directly from Submicron-Sized Iron Grains by Thermal Evaporation. *Phys. Rev. B* **2004**, *70*, 233404.

(13) Breaux, G. A.; Benirschke, R. C.; Sugai, T.; Kinnear, B. S.; Jarrold, M. F. Hot and Solid Gallium Clusters: Too Small to Melt. *Phys. Rev. Lett.* **2003**, *91*, 215508.

(14) Wu, Y.; Yang, P. Melting and Welding Semiconductor Nanowires in Nanotubes. *Adv. Mater.* **2001**, *13*, 520−523.

(15) Lai, S. L.; Guo, J. Y.; Petrova, V.; Ramanath, G.; Allen, L. H. Size-Dependent Melting Properties of Small Tin Particles: Nanocalorimteric Measurement. *Phys. Rev. Lett.* **1996**, *77*, 99−102.

(16) Wang, X. W.; Fei, G. T.; Zheng, K.; Jin, Z.; Zhang, L. D. Size-Dependent Melting Behavior of Zn Nanowire Arrays. *Appl. Phys. Lett.* **2006**, *88*, 173114.

(17) Takagi, M. Electron-Diffraction Study of Liquid-Solid Transition of Thin Metal Films. *J. Phys. Soc. Jpn.* **1954**, *9*, 359−363.

(18) Lee, S.; Oshima, Y.; Hosono, E.; Zhou, H.; Kim, K.; Chang, H. M.; Kanno, R.; Takayanagi, K. In Situ TEM Observation of Local Phase Transformation in a Rechargeable $LiMn_2O_4$ Nanowire Battery. *J. Phys. Chem. C* **2013**, *117*, 24236−24241.

(19) Chen, K. C.; Wu, W. W.; Liao, C. N.; Chen, L. J.; Tu, K. N. Observation of Atomic Diffusion at Twin-Modified Grain Boundaries in Copper. *Science* **2008**, *321*, 1066−1069.

(20) Lu, K. C.; Wu, W. W.; Wu, H. W.; Tanner, C. M.; Chang, J. P.; Chen, L. J.; Tu, K. N. In situ Control of Atomic-Scale Si Layer with Huge Strain in the Nanoheterostructure NiSi/Si/NiSi through Point Contact Reaction. *Nano Lett.* **2007**, *7*, 2389−2394.

(21) Kallesøe, C.; Wen, C. Y.; Booth, T. J.; Hansen, O.; Bøggild, P.; Ross, F. M.; Mølhave, K. In Situ TEM Creation and Electrical Characterization of Nanowire Devices. *Nano Lett.* **2012**, *12*, 2965−2970.

(22) Tanaka, T.; Saito, K.; Nishio, M.; Guo, Q.; Ogawa, H. Enhanced Light Output from ZnTe Light Emitting Diodes by Utilizing Thin Film Structure. *Appl. Phys. Express* **2009**, *2*, 122101.

(23) Schrier, J.; Demchenko, D. O.; Wang, L. W. Optical Properties of ZnO/ZnS and ZnO/ZnTe Heterostructures for Photovoltaic Applications. *Nano Lett.* **2007**, *7*, 2377−2382.

(24) Wu, Q.; Litz, M.; Zhang, X. C. Broadband Detection Capability of ZnTe Electro-Optic Field Detectors. *Appl. Phys. Lett.* **1996**, *68*, 2924−2926.

(25) Liu, Z.; Chen, G.; Liang, B.; Yu, G.; Huang, H.; Chen, D.; Shen, G. Fabrication of High-Quality ZnTe Nanowires Toward High-Performance Rigid/Flexible Visible-Light Photodetectors. *Opt. Express* **2013**, *21*, 7799−7810.

(26) Mingo, N. Erratum: Thermoelectric Figure of Merit of II−VI Semiconductor Nanowires. *Appl. Phys. Lett.* **2004**, *85*, 5986−5988.

(27) Davami, K.; Kang, D.; Lee, J. S.; Meyyappan, M. Synthesis of ZnTe Nanostructures by Vapor−Liquid−Solid Technique. *Chem. Phys. Lett.* **2011**, *504*, 62−66.

(28) Kirmse, H.; Neumann, W.; Kret, S.; Dluzewski, P.; Janik, E.; Karczewski, G.; Wojtowicz, T. TEM Characterization of VLS-Grown ZnTe Nanowires. *Phys. Status Solidi C* **2008**, *5*, 3780−3784.

(29) Ahn, C. C.; Krivanek, O. L.; Burgner, R. P.; Disko, M. M.; Swann, P. R. *EELS Atlas*; Center for Solid State Science, Arizona State University: Tempe, AZ, 1983.

(30) Huang, C. W.; Hsin, C. L.; Wang, C. W.; Chu, F. H.; Kao, C. Y.; Chen, J. Y.; Huang, Y. T.; Lu, K. C.; Wu, W. W.; Chen, L. J. Direct Observation of Melting Behaviors at the Nanoscale Under Electron Beam and Heat to Form Hollow Nanostructures. *Nanoscale* **2012**, *4*, 4702−4706.

(31) Klabunde, K. J. *Nanoscale Materials in Chemistry*; John Wiley & Sons, Inc.: Hoboken, NJ, 2001.

(32) Wautelet, M. Estimation of the Variation of the Melting Temperature with the Size of Small Particles, on the Basis of a Surface-Phonon Instability Model. *J. Phys. D: Appl. Phys.* **1991**, *24*, 343−346.

(33) Nanda, K. K.; Sahu, S. N.; Behera, S. N. Liquid-Drop Model for the Size-Dependent Melting of Low-Dimensional Systems. *Phys. Rev. A* **2002**, *66*, 013208.

(34) Pawlow, P. The Dependency of the Melting Point on the Surface Energy of a Solid Body. *Z. Phys. Chem.* **1909**, *65*, 545−548.

(35) Borel, J. P. Thermodynamical Size Effect and the Structure of Metallic Clusters. *Surf. Sci.* **1981**, *106*, 1−9.

(36) Quyang, G.; Li, X. L.; Tan, X.; Yang, G. W. Surface Energy of Nanowires. *Nanotechnology* **2008**, *19*, 045709.

(37) Quyang, G.; Tan, X.; Yang, G. W. Thermodynamic Model of the Surface Energy of Nanocrystal. *Phys. Rev. B* **2006**, *74*, 195408.

(38) Quyang, G.; Zhu, Z. M.; Zhu, W. G.; Sun, C. Q. Size Dependent Debye Temperature and Total Mean Square Relative Atomic Displacement in Nanosolids under High Pressure and High Temperature. *J. Phys. Chem. C* **2010**, *114*, 1805−1808.

(39) Sun, C. Q.; Wang, Y.; Tay, B. K.; Li, S.; Huang, H.; Zhang, Y. B. Correlation between the Melting Point of a Nanosolid and the

Cohesive Energy of a Surface Atom. *J. Phys. Chem. B* **2002**, *106*, 10701−10705.
(40) Sun, C. Q.; Sun, Y.; Ni, Y.; Zhang, X.; Pan, J.; Wang, X. H.; Zhou, J.; Li, L. T.; Zheng, W.; Yu, S.; Pan, L. K.; Sun, Z. Coulomb Repulsion at the Nanometer-Sized Contact: A Force Driving Superhydrophobicity, Superfluidity, Superlubricity, and Supersolidity. *J. Phys. Chem. C* **2009**, *113*, 20009−20019.